

Patterned loading of a Bose-Einstein condensate into an optical lattice

S. Peil,¹ J. V. Porto,¹ B. Laburthe Tolra,¹ J. M. Obrecht,¹ B. E. King,¹ M. Subbotin,² S. L. Rolston,¹ and W. D. Phillips¹

¹National Institute of Standards and Technology, Gaithersburg, Maryland 20899

²Institute of Spectroscopy RAS, Troitsk, Moscow Region, 142092, Russia

(Received 19 September 2002; published 28 May 2003)

We have developed a technique to control the placement of atoms in an optical lattice by using a superlattice comprising two separately manipulated, periodic optical potentials with commensurate periods. We demonstrate selective loading of Bose-condensed ⁸⁷Rb atoms into every third site of a one-dimensional optical lattice. Our technique provides atoms with wide separation yet tight confinement, useful properties for neutral-atom implementations of quantum computing. Interference of atoms released from the optical lattice and optical Bragg reflection from the atoms reveal the tight confinement and wide separation provided by the patterned filling.

DOI: 10.1103/PhysRevA.67.051603

PACS number(s): 03.75.Hh, 39.25.+k, 03.67.Lx

Neutral atoms confined in an array of magnetic or optical traps offer a scalable system for quantum information processing. Several proposals [1–3] for providing the required coherent control of the states of individual atoms and their interactions involve optical lattices, periodic light-shift potentials produced by optical standing waves. Ideally, the lattice should be able to separate the atoms (qubits) by more than an optical wavelength (to allow individual optical addressing) while confining each atom to a region much smaller than an optical wavelength. Tight confinement is important in most of these proposals both to increase the interaction strength between atoms in a site [1,2] and to decrease the oscillation period, which sets the time scale for moving atoms.

Here we experimentally demonstrate a technique to selectively load atoms into the motional ground state of every third site of a one-dimensional (1D) optical lattice. This technique involves the sequential application of two independent lattices whose spatial periods differ by a factor of 3. We use the resulting “superlattice” to transfer atoms in a Bose-Einstein condensate (BEC) from the long-period lattice sites to the coinciding sites of the short-period lattice. The final state provides the tight confinement of the short-period lattice with a separation three times larger than the lattice period. Large separation between sites can also be achieved by using CO₂ lasers [4] or arrays of optical dipole traps [5], but these techniques require much more laser power to provide similar confinement. Patterned loading adds versatility to the atom-lattice architecture, and empty sites between atoms are in fact necessary for quantum computing proposals such as Ref. [1]. While the present experiment involves many atoms in every third plane of a single 1D lattice site, the technique can be extended to other fractional fillings and to 3D lattices, which could have single atoms in individual sites.

We create each of the lattices by intersecting two laser beams at an angle θ_i (see Fig. 1). The lattice period $d_i = \lambda/[2 \sin(\theta_i/2)]$, where $\lambda = 2\pi/k$ is the laser wavelength. In this experiment, the θ_i are chosen such that the periods differ by a factor of 3, resulting in parallel lattices with periods of $d_l = 1.5 \mu\text{m}$ (long lattice) and $d_s = 0.5 \mu\text{m}$ (short lattice). The light-shift potential is given by

$$U(z) = -\frac{U_l}{2} \cos(2\pi z/d_l) - \frac{U_s}{2} \cos(2\pi z/d_s + \phi). \quad (1)$$

We express U in units of the atomic recoil $E_R = \hbar^2 k^2 / (2M)$, where M is the atomic mass. Given the periodic nature of $U(z)$, the eigenstates of this system are Bloch states. It is important that the two lattices be sufficiently commensurate that the local relative phase between the two lattices does not change significantly along the BEC. We achieve this with a ratio d_l/d_s of 2.99(1) [6], as determined by measuring the Talbot time [7] for each lattice, $T = \hbar/\epsilon_{R_i}$, where $\epsilon_{R_i} = (\hbar^2 k^2 / 2M)(\lambda/d_i)^2$ is the lattice recoil energy. (Following diffraction from a brief application of lattice light, the evolution of the wave function is periodic with period T .)

The source of our lattice light is a Ti:sapphire laser detuned below the $D2$ line of Rb (780 nm) by ~ 100 GHz. Each beam has up to 3 mW in a waist ($1/e^2$ radius) of

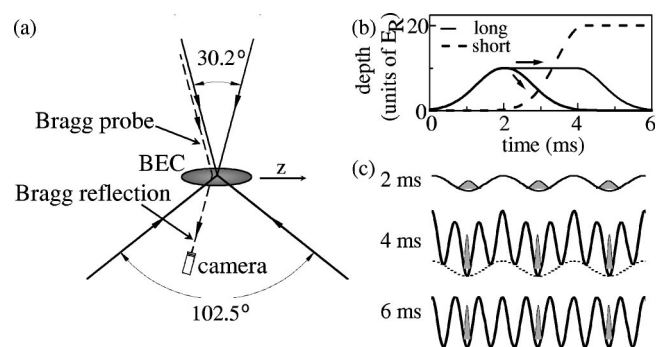


FIG. 1. (a) Superlattice arrangement. Two pairs of laser beams form two independent 1D lattices, with period ratio 3:1. A beam incident at the Bragg condition for the long-lattice period probes the atomic density distribution. The plane containing the long-lattice beams (intersecting at 30.2°) is at 75° to the (horizontal) plane of the short-lattice beams. (b) Example of time sequences for loading every third site of the short lattice. The lattices can be loaded sequentially or the long lattice can be removed while the short lattice is applied. (c) Schematic of atom localization for sequential loading: in the long lattice (at 2 ms), superlattice (4 ms), and finally the desired state in the short lattice (6 ms).

250 μm , giving a depth $U_i < 60E_R$ and a spontaneous emission rate $< 10 \text{ s}^{-1}$. Separate acousto-optic modulators allow independent control of the two lattices. In order to ensure independent lattices, we detune them from each other by 60 MHz [8]. The relative position of the minima of the two lattices, determined by ϕ , is not locked. Interferometric measurements showed this phase moved by less than a radian during a given loading cycle ($\leq 10 \text{ ms}$ duration), although it is random between cycles.

Our BECs are produced in a Ioffe-Pritchard trap every 30 s. In the first 4 s, 10^9 ^{87}Rb atoms from a Zeeman-slowed beam are collected in a magneto-optical trap (MOT). The MOT magnetic fields are then turned off, the atoms cooled for 6 ms in optical molasses to $\sim 40 \mu\text{K}$, optically pumped into either the $|F, m_F\rangle = |2, 2\rangle$ or $|F, m_F\rangle = |1, -1\rangle$ hyperfine state, and finally captured in a roughly spherical magnetic trap whose strength is chosen to match the initial size of the atom cloud. Compression over 4 s produces a trap with axial frequency for $|F, m_F\rangle = |2, 2\rangle$ ($|1, -1\rangle$) atoms of $\nu_z = 12 \text{ Hz}$ (9 Hz) and radial frequency of $\nu_\rho = 380 \text{ Hz}$ (270 Hz). Forced RF evaporation for 20 s cools the atoms below the BEC transition producing a condensate with no discernible thermal component. We then weaken the radial magnetic trap to $\nu_\rho = 36 \text{ Hz}$ (26 Hz). A typical condensate has $\sim 2 \times 10^5$ atoms and a Thomas-Fermi length [9] of 55 μm in the lattice direction, occupying ~ 110 (37) sites of the short (long) lattice.

Atom diffraction provides information about the confinement and periodicity of atoms in our lattice, and direct spatial imaging of the patterned state is not possible with our current imaging resolution. After abruptly turning off the lattice light ($< 1 \mu\text{s}$) and magnetic trap ($< 200 \mu\text{s}$) we allow the atoms to freely expand for 22 ms before absorption imaging the resulting atomic interference [10]. This produces a diffraction pattern that corresponds to the absolute square of the Fourier transform of the BEC's spatial wave function in the lattice, i.e., the momentum distribution. If the spatial wave function is periodic with period d its momentum components are restricted to multiples of $\pm h/d$. The width at each site, Δz , determines the width of the envelope of the momentum distribution, $\Delta p \approx \hbar/\Delta z$.

Figure 2 shows atom-diffraction patterns obtained from loading atoms into the (a) long lattice and (b) short lattice. To load an individual lattice we turn on the lattice beams with a half-Gaussian ramp, adiabatically with respect to vibrational excitations within the lattice sites. (The time scales for adiabaticity are discussed below.) Comparing Fig. 2(a) with 2(b), the separations between the momentum peaks have a ratio of 1:3, corresponding to the 3:1 ratio of the respective lattice periods. The amplitudes of the momentum peaks for a single lattice are solely determined by the ratio U_i/ϵ_{R_i} of the lattice depth to the lattice recoil energy. Since $\epsilon_{R_i} \propto 1/d_i^2$, $\epsilon_{R_s}/\epsilon_{R_l} = 9$. The short lattice in Fig. 2(b) has nine times higher intensity than the long lattice in Fig. 2(a), so the diffraction patterns have peaks with the same relative heights. The tighter confinement in the short lattice gives the three times wider diffraction pattern.

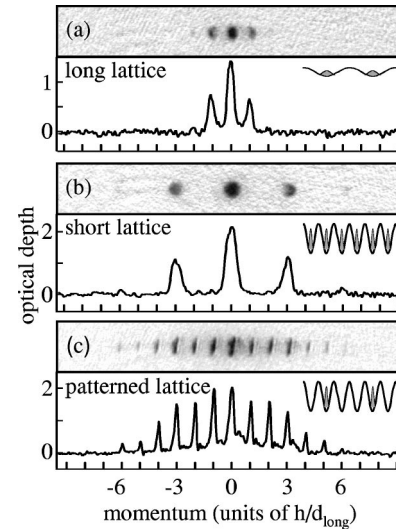


FIG. 2. Single shot absorption images and their line profiles showing atom-diffraction patterns from $|1, -1\rangle$ atoms loaded into (a) the long lattice, (b) the short lattice, and (c) every third site of the short lattice. The long- and short-lattice depths are roughly $2E_R$ and $20E_R$, respectively. [The narrowing of the diffraction peaks is the result of a lensing effect due to the nonuniform intensity distribution of the lattice beams along the lattice, resulting in a quadratic phase variation of the wave function. This effect is most visible in loading sequence (c), in which the phase is integrated for three times longer than in (a) and (b).]

To load every third site of the short lattice, we apply the lattices to the BEC as shown in Fig. 1(b). First, the long lattice is slowly turned on to localize the atoms at its lattice sites. The short lattice is then slowly added, localizing the atoms at those of its lattice sites that are closest to the longer period ones. These operations are adiabatic with respect to vibrational excitation and atoms go from the ground state of the long lattice to the ground state of the superlattice. Slowly turning off the long lattice leaves the atoms well localized in every third site of the short lattice. Alternatively, the loading procedure can be performed more quickly by simultaneously removing the long lattice while turning on the short lattice.

The final state in either procedure is an equal superposition of the three Bloch states in the first band of the short lattice with quasimomentum $q = 0, \pm 1/3$. This state leads to a diffraction image like Fig. 2(c) (which was taken using the latter procedure). As expected, the peak spacings for the pattern-loaded short lattice are indicative of the long-lattice periodicity. The tight confinement of the short lattice produces the broad envelope of the diffraction pattern, which we verified increases with short lattice depth. We obtain the same confinement and spontaneous emission rate with $(d_l/d_s)^4 = 81$ times less power and $(d_l/d_s)^2 = 9$ times smaller detuning than would be necessary using the long lattice alone. In a practical quantum computing application, both the detuning and (d_l/d_s) would be larger than our chosen experimental parameters, further increasing the benefit of the patterned loading technique.

Surprisingly, atom diffraction is insensitive to tunneling from occupied to empty sites: the evolution of the patterned state consists entirely of phase evolution of the three quasi-

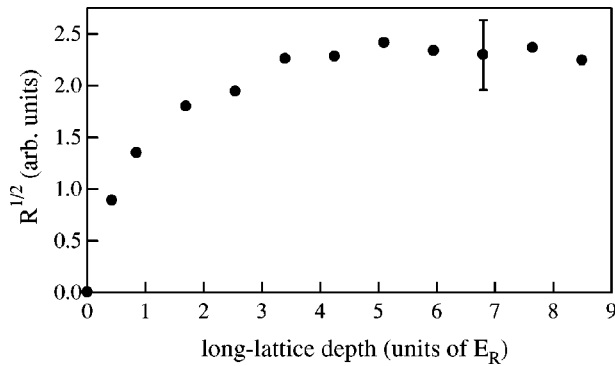


FIG. 3. Square root of the Bragg reflection, $R^{1/2}$, from pattern-loaded $|2,2\rangle$ atoms vs the maximum U_l used in the sequential loading sequence. (The final $U_s = 12E_R$.) The Bragg probe beam was a $3\text{-}\mu\text{s}$ pulse of 1 mW in a $300\text{-}\mu\text{m}$ waist ($1/e^2$), detuned seven linewidths below resonance.

momentum components, which project onto completely independent plane-wave states. To verify that we have indeed loaded every third site, we use optical Bragg diffraction [11] (reflection of a probe beam from a periodic array of atoms). The reflected signal is proportional to the square of the Fourier-transform component of the atomic density at the spatial frequency satisfying the Bragg condition. We apply the probe beam along one of the long-lattice beams and detect along the other (see Fig. 1), after switching off the lattice beams. This geometry satisfies the first-order Bragg condition for density modulations with period d_l , with no reflection for density modulations of period d_s .

We look for Bragg reflection in four situations: BEC only, loading into the short lattice, loading into the long lattice, and loading into the short lattice with our patterned-loading procedure. We detect no reflection from either the BEC or the atoms loaded directly into the short lattice. When atoms are loaded into the long lattice we see substantial reflectivity (of order 100%, but a quantitative determination is difficult). We observe essentially the same signal from atoms pattern loaded into the short lattice [using either procedure shown in Fig. 1(b)], consistent with all of the atoms being loaded into every third site. While it is difficult to quantify the fraction of atoms put into every third site, we see in Fig. 3 that the square root of the Bragg reflection (proportional to the “every third” fraction) saturates with increasing U_l . This saturation and the comparable Bragg reflectivity of the long lattice and pattern-loaded short lattice support the conclusion of complete loading into every third site.

The issue of adiabaticity is complicated for our superlattice. We want the loading process to avoid any vibrational excitations. On the other hand, our desired final state (only every third short-lattice site occupied) is not the ground state of the system (every lattice site occupied). We must, in fact, be fast (fully *nonadiabatic*) with respect to the time to tunnel between sites of the short lattice. To investigate adiabaticity, we applied different sequences of lattice light to the BEC and observed the resulting atom diffraction. The experiments are summarized in Fig. 4. If the atoms follow the ground state throughout a given sequence, they will return to the original BEC when all lattice light is removed. Such adiabaticity re-

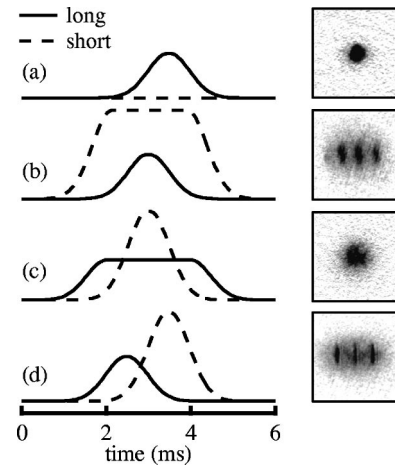


FIG. 4. Investigation of adiabaticity for several loading sequences (see text). The schematic traces on the left indicate the lattice depths as a function of time, where the peak depths are $5E_R$ and $12E_R$ for the long and short lattices. The images on the right are the corresponding absorption images, in which nonadiabaticity appears as momentum components spaced at h/d_l .

quires that the time-dependent lattice Hamiltonian $H(t)$ satisfy

$$\hbar \dot{U}_i \frac{\langle m | \frac{dH}{dU_i} | 0 \rangle}{(E_m - E_0)^2} \ll 1 \quad (2)$$

for all states $|m\rangle$ with energy E_m coupled to the ground state by $H(t)$ [12,13]. For a single lattice the most stringent requirement, which occurs at $U_i=0$, is $\hbar \dot{U}_i \ll 2\sqrt{2}\epsilon_{R_i}^2$ (as determined by a band-structure calculation). Figure 4(a) shows the BEC after loading and unloading a $5E_R$ -deep long lattice with a Gaussian pulse ($\sigma=0.3\text{ ms}$). We satisfy the adiabatic criterion by a factor of 25, and the final state shows no sign of excitations. Experiments with a Na BEC reported greater than 99% of the population loaded into the ground vibrational state with a similar procedure [14].

In case 4(b), we adiabatically load the short lattice, apply the long lattice, and then reverse the procedure. This process is clearly not adiabatic, as evidenced by the momentum peaks associated with the long lattice. When the long lattice turns on, the period of the combined lattice changes from $0.5\text{ }\mu\text{m}$ to $1.5\text{ }\mu\text{m}$. To adiabatically follow this change requires tunneling between short lattice sites, which is quite slow ($\sim 60\text{ ms}$ for our $12E_R$ deep lattice).

In Fig. 4(c) we reversed the roles of the long and short lattices compared to Fig. 4(b). While superficially similar to Fig. 4(b), Fig. 4(c) is by contrast adiabatic, as evidenced by the lack of diffraction peaks. Here the periodicity of the combined lattice remains $1.5\text{ }\mu\text{m}$ throughout, and the atoms do not have to tunnel to follow the ground state. This picture shows that we can adiabatically load the ground state of the superlattice. While the resolution in Fig. 4(c) does not allow us a precise determination of the degree of adiabaticity, band-structure calculations show that we satisfy the adiabaticity criterion.

ticity criterion [Eq. (2)] by more than a factor of 25, implying superlattice ground state population of more than 99.8% [12].

Figure 4(d) is the patterned-loading sequence followed by an adiabatic turn off of the short lattice. As expected the patterned state (a superposition of Bloch states) is not the ground state. We note that the momentum distribution due to sudden shut off of the lattice in Fig. 2(c) represents the plane-wave decomposition of the patterned wave function in the lattice, while Fig. 4(d) shows those plane-wave states that adiabatically connect to the populated Bloch states in the lattice.

We have performed band-structure calculations, evaluating the adiabatic criteria of Eq. (2), to investigate the effect of the relative phase ϕ between the short and long lattices, which is uncontrolled in the experiment. We find that except for a very narrow range near $\phi = \pi$, where the superlattice is a periodic array of double well potentials, the loading sequence produces the desired state with every third site

loaded. The calculation also confirmed that the measured temporal variations of ϕ do not significantly compromise the loading process. Stabilizing the relative phase should be straightforward, and would allow the study of the double-well system, for example.

The combination of patterned loading and optical Bragg reflection presents a unique opportunity for future investigation of tunneling from an occupied site to an empty site, a process that should be inhibited by mean-field interactions (“macroscopic quantum self-trapping” [15]). Similar inhibition of tunnelling leads to the Mott insulator transition as observed in Ref. [16] in a uniformly filled 3D lattice. Combining the Mott transition with our patterned loading technique extended to 3D should provide a flexible system for the implementation of quantum computing with atoms in optical lattices.

This work was funded by ARDA. M.S. acknowledges support from the U.S. Civilian Research and Development Foundation, Grant No. RP1-2261, and the Russian Foundation for Fundamental Research, Grant No. 01-02-16337.

-
- [1] D. Jaksch *et al.*, Phys. Rev. Lett. **82**, 1975 (1999).
 [2] G.K. Brennen, C.M. Caves, P.S. Jessen, and I.H. Deutsch, Phys. Rev. Lett. **82**, 1060 (1999).
 [3] D. Jaksch *et al.*, Phys. Rev. Lett. **85**, 2208 (2000).
 [4] R. Scheunemann, F.S. Cataliotti, T.W. Hänsch, and M. Weitz, Phys. Rev. A **62**, 051801(R) (2000).
 [5] R. Dumke *et al.*, Phys. Rev. Lett. **89**, 097903 (2002).
 [6] All uncertainties reported here are one standard deviation combined statistical and systematic uncertainties.
 [7] L. Deng *et al.*, Phys. Rev. Lett. **83**, 5407 (1999).
 [8] The atoms’ response to the high-frequency interference between the two lattices is negligible.
 [9] F. Dalfovo, S. Giorgini, L.P. Pitaevskii, and S. Stringari, Rev. Mod. Phys. **71**, 463 (1999).
 [10] Yu. B. Ovchinnikov *et al.*, Phys. Rev. Lett. **83**, 284 (1999).
 [11] G. Birkl *et al.*, Phys. Rev. Lett. **75**, 2823 (1995).
 [12] See, for example, L. Schiff, *Quantum Mechanics* (McGraw-Hill, New York, 1955).
 [13] For a harmonic oscillator Hamiltonian $U_i x^2$, this reduces to $\dot{\omega}_m \ll \omega_m^2$.
 [14] J. Hecker Denschlag *et al.*, J. Phys. B **35**, 3095 (2002).
 [15] A. Smerzi, S. Fantoni, S. Giovanazzi, and S.R. Shenoy, Phys. Rev. Lett. **79**, 4950 (1997).
 [16] M. Greiner *et al.*, Nature (London) **415**, 39 (2002).